Earth and Planetary Science Letters 295 (2010) 477–486

Contents lists available at ScienceDirect

Earth and Planetary Science Letters

journal homepage: www.elsevier.com/locate/epsl

Thermodynamics of mixing in $MgSiO_3$–Al_2O_3 perovskite and ilmenite from ab initio calculations

D.Y. Jung [a,*], V.L. Vinograd [b], O.B. Fabrichnaya [c], A.R. Oganov [d,e], M.W. Schmidt [f], B. Winkler [b]

[a] Laboratory of Crystallography, ETH Zurich, Wolfgang-Pauli-Strasse 10, CH-8093 Zurich, Switzerland
[b] Institute of Geosciences, University of Frankfurt, Altenhoeferallee 1, 60438 Frankfurt a. M., Germany
[c] TU Bergakademie Freiberg, Institut für Werkstoffwissenschaft, Gustav-Zeuner-Strasse 5, 09599 Freiberg, Germany
[d] Department of Geosciences, Department of Physics and Astronomy, and New York Center for Computational Sciences, Stony Brook University, Stony Brook NY 11794-2100, USA
[e] Geology Department, Moscow State University, 119992 Moscow, Russia
[f] Institute for Mineralogy and Petrology, Clausiusstrasse 5, 8092 Zurich, Switzerland

ARTICLE INFO

Article history:
Received 2 October 2009
Received in revised form 12 April 2010
Accepted 15 April 2010
Available online 20 May 2010

Editor: L. Stixrude

Keywords:
ab initio
double defect method
cluster expansion
thermal modeling
solid solutions

ABSTRACT

The thermodynamic mixing functions of $MgSiO_3$–Al_2O_3 solid solutions in perovskite and ilmenite structures were modeled based on the results of ab initio calculations applied to a set of supercell structures containing 64 and 48 exchangeable sites, respectively. The sampled structures were constructed from the supercells of the end-members $MgSiO_3$ perovskite and Al_2O_3 corundum by inserting double AlAl and MgSi defects, respectively, at all possible distances. From these calculations the pairwise effective interactions were derived and used to calculate enthalpy differences between successive configurations produced in Monte Carlo simulation runs. The temperature dependent enthalpies of mixing of the solid solutions were evaluated as averages over the Monte Carlo runs while the free energies of mixing were calculated with the method of thermodynamic integration. The phase equilibria of perovskite, ilmenite and garnet in the Mg–Si–Al–O system were calculated using the computed models of mixing and the standard thermodynamic properties of the end-members from the data base of Fabrichnaya (1999). The obtained activity–composition models are in good agreement with available experimental constraints, thereby showing that the thermodynamic effects of mixing in silicate solid solutions with coupled substitutions can be reliably predicted based on ab initio calculated total energies of a small set of supercell structures.

1. Introduction

Phase equilibria in the Mg–Al–Si–O (MAS) system at high pressures and temperatures form a reference frame which is important for interpreting seismic discontinuities in the Earth's mantle. The experimental and theoretical analysis of MAS is complicated due to the poorly known thermodynamics of mixing of $MgSiO_3$–Al_2O_3 solid solutions in typical mantle minerals. For example, the equilibrium between perovskite, ilmenite and garnet, which might be responsible for the 660 km seismic discontinuity, is very sensitive to the fractions of Al_2O_3 and $MgSiO_3$ components in the system (Irifune et al., 1996; Kubo and Akaogi, 2000; Hirose et al., 2001). Recent theoretical (Yamamoto et al., 2003; Akber-Knutson and Bukowinski, 2004; Zhang and Oganov, 2006) and experimental studies (Stebbins et al., 2003;Walter et al., 2006) seem to agree that the substitution of alumina into the Mg silicates occurs via the charge-coupled mechanism, MgSi = 2Al. Due to the limited range of investigated Al_2O_3 concentrations in perovskite and ilmenite, it is difficult to assess thermodynamic mixing parameters of these solid solutions solely on the basis of the available experimental data. Moreover, the coupled substitution involving the cations of different charge and size precludes the use of simple thermodynamic mixing models. Recently, Panero et al. (2006) have estimated the enthalpy of mixing in the $MgSiO_3$–Al_2O_3 solid solutions in perovskite and ilmenite based on ab initio calculations of excess enthalpies of several supercell structures with various Al/Mg ratios. Their results achieved within the assumption of regular model suggested that the degree of non-ideality of mixing in the perovskite phase is smaller than in the ilmenite phase. Here the conclusions of Panero et al. (2006) are tested against DFT calculations performed on a more extensive set of supercell structures. The present set of the supercell structures is selected on the basis of the double defect method (DDM) (Hoshino et al., 1993; Vinograd et al., 2009), which has been recently successfully applied to modeling the effects of ordering and mixing in the solid solution between calcite, $CaCO_3$, and magnesite, $MgCO_3$ (Vinograd et al., 2009). Here the DDM is extended to the case of MgSi = 2Al substitution, where the mixing occurs on two sublattices. Monte Carlo simulations based on the DFT results are used to map the temperature-dependent thermodynamic mixing properties of $MgSiO_3$–Al_2O_3 solid solutions with ilmenite and perovskite structures and to investigate deviations

* Corresponding author. Tel.: +41 44 633 71 38; fax: +41 44 632 1133.
E-mail address: daniel.jung@mat.ethz.ch (D.Y. Jung).

0012-821X/$ – see front matter © 2010 Elsevier B.V. All rights reserved.
doi:10.1016/j.epsl.2010.04.026

from regular behaviour. The obtained models of mixing together with the model of pyrope–majorite solid solution developed earlier (Vinograd et al., 2006) and the assessed standard thermodynamic properties of the end-members of perovskite, ilmenite and garnet (Fabrichnaya, 1999) are used to predict phase equilibria in MAS in the pressure range of 20–30 GPa and in the temperature range of 1773–2273 K.

2. DDM vs. random sampling

Recent progress in simulation studies of solid solutions was stimulated by the development of methods of effective parameterization of the excess enthalpy. It has been shown that the excess enthalpies of various supercell structures in a solid solution can be accurately expanded in terms of energetic contributions from clusters of different size and shape (Connolly and Williams, 1983; Sanchez et al., 1984). In mineralogical studies the excess enthalpy of solid solution phases has been often parameterized in terms of the contributions from pair clusters only (Becker et al., 2000; Bosenick et al., 2000; Warren et al., 2001; Becker and Pollok, 2002; Vinograd et al., 2004; Vinograd and Sluiter, 2006; Vinograd et al., 2006, 2007a,b; Palin and Harrison, 2007). The success of the simplified expansion method is based on the notion that the typical applications in mineralogical studies were concerned with oxides, where the interactions between the exchangeable atoms (the cations) are mediated by "inert" oxygen atoms, thereby decreasing importance of many-body effects (Vinograd et al., 2009). When many-body interactions can be ignored, the excess enthalpy of any configuration of a binary $A_xB_{1-x}R$ solution can be written:

$$\Delta H = \sum_n f_{AB}^{(n)} J_{AB}^{(n)}, \tag{1}$$

where $f_{AB}^{(n)}$ is the number of AB and BA pairs at the n-th distance within a supercell and $J_{AB}^{(n)}$ is the enthalpy effect of the intracrystalline reaction AA + BB = 2AB, where the pairs of the exchangeable atoms are considered at the same distance n within the lattice. Typically the Js are assumed to be configuration independent. Therefore, $J_{AB}^{(n)}$ is the effective interaction at the distance n. When the Js are known the temperature dependent properties such as the enthalpy, entropy and Gibbs free energy of mixing can be reliably computed with the Monte Carlo method (Bosenick et al., 2000; Warren et al., 2001).

The usual approach to the evaluation of the Js is to calculate the excess enthalpies and $f_{AB}^{(n)}$ for several hundred of randomly varied configurations and to apply a least squares fit. The calculation of the excess enthalpies of several hundred supercell structures is usually a formidable task, therefore, force-field approaches have been often employed. Recently, it has been shown that the number of the supercell structures to be tested can be greatly reduced when the configurations are selected based on a deterministic principle, namely the DDM (Hoshino et al., 1993; Vinograd et al., 2009). The structures required for the DDM calculations are constructed from the supercells of the end-members AR and BR by inserting double defects of BB and AA types, respectively, at all possible interatomic distances. In supercells of reasonable size (~1000 Å^3) the number of such distances does not exceed 10–20, so that about 20–40 structures are to be processed.

The double defect method (DDM) is based on the notion (Hoshino et al., 1993) that in the composition limit of the end-member AR the effective pair interactions in a binary $(A_xB_{1-x})R$ solid solution can be calculated with the equation

$$J_{AB/A}^{(n)} = H_{AB}^{(n)} + H_{BA}^{(n)} - H_{AA}^{(n)} - H_{BB}^{(n)} \tag{2}$$

where $H_{ij}^{(n)}$ is the total energy of a supercell structure prepared from pure "A" composition by inserting an IJ pair at the distance n. One notes also that the A atoms, which belong to the pairs, are indistinguishable from the A atoms of the matrix. Hence, the AA pair disappears, while the AB and BA pairs reduce to single B-type defects within the A-matrix. Therefore Eq. (2) can be written in more simply as

$$J_{AB/A}^{(n)} = 2H_B - H(A) - H_{BB}^{(n)}, \tag{3}$$

where $J_{AB/A}^{(n)}$ is the pair ECI at the distance n in the limit of pure "A", H_B and $H_{BB}^{(n)}$ are the enthalpies of the supercells with single B- and double BB-defects, respectively and H(A) is the enthalpy of pure "A" supercell. By adding and subtracting twice the energy of the mechanical mixture $2(H(A)x_A + H(B)x_B)$ to the right-hand side of Eq. (3), where $x_B = 1/N$ and N is the number of sites in the supercell, Eq. (3) can be rewritten in terms of the excess properties of the supercells (Vinograd et al., 2009)

$$J_{AB/A}^{(n)} = 2\Delta H_B - \Delta H_{BB}^{(n)}. \tag{4}$$

Here ΔH_B and $\Delta H_{BB}^{(n)}$ are the excess enthalpies of the supercells with single B- and double BB-defects, respectively. Similarly, in the B-limit

$$J_{AB/B}^{(n)} = 2\Delta H_A - \Delta H_{AA}^{(n)}. \tag{5}$$

In the case of periodic boundary conditions Eqs. (4) and (5) transform as follows

$$J_{AB/A}^{(n)} = \left(2\Delta H_B - \Delta H_{BB}^{(n)}\right)/D_n, \tag{6}$$

$$J_{AB/B}^{(n)} = \left(2\Delta H_A - \Delta H_{AA}^{(n)}\right)/D_n, \tag{7}$$

where D_n is the degeneracy factor, which is an integer typically found in the range of 1–8. Further considerations (Vinograd et al., 2009) permit to substitute $2\Delta H_B$ and $2\Delta H_A$ terms in Eqs. (6) and (7) with the effective parameters $\Delta H_{BB}^{(\infty)}$ and $\Delta H_{AA}^{(\infty)}$ which have the meaning of the energies of hypothetical supercells with the pairs of defects at infinite separation:

$$J_{AB/A}^{(n)} = \left(\Delta H_{BB}^{(\infty)} - \Delta H_{BB}^{(n)}\right)/D_n, \tag{8}$$

$$J_{AB/B}^{(n)} = \left(\Delta H_{AA}^{(\infty)} - \Delta H_{AA}^{(n)}\right)/D_n. \tag{9}$$

The values of these parameters are obtained from the fit to the excess energies of the single- and double-defect structures via Eq. (1). The two sets of the Js characterize the pair ECIs at two extremes along the composition axis. The variation of the Js at intermediate compositions is assumed to be a linear combination of the Js calculated in A- and B-limits:

$$J_{AB}^{(n)} = x_A J_{AB/A}^{(n)} + x_B J_{AB/B}^{(n)}. \tag{10}$$

The DDM has been successfully applied to predict phase relations in the calcite–magnesite system (Vinograd et al., 2009) where a $3\times3\times1$ supercell of $R\bar{3}c$ calcite ($a = 14.964$ Å, $c = 17.061$ Å) containing 54 exchangeable sites was considered. The enthalpies of the single- and double-defect structures were calculated using the force-field model of Austen et al. (2005) and the program GULP (Gale, 1997; Gale and Rohl, 2003). The calculations permitted a nearly quantitative description of the experimental subsolidus phase diagram (Goldsmith and Heard, 1961).

Here the DDM is extended to a more complex case of a coupled substitution $A_\alpha C_\beta = B_\alpha D_\beta$, where the mixing occurs on two sublattices.

While in an $(A_xB_{1-x})R$ solid solution there is only one ordering reaction of AA + BB = 2AB type, in the case of a coupled substitution one needs to consider three ordering reactions, namely AA + BB = 2AB and CC + DD = 2CD, which occur within α and β sublattices, respectively, and the cross-sublattice interaction AC + BD = AD + BC. The excess enthalpy per supercell of a binary $(AC)_x(BD)_{1-x}R$ solution can be written:

$$\Delta H = \sum_n f_{AB}^{(n)} J_{AB}^{(n)} + \sum_k f_{CD}^{(k)} J_{CD}^{(k)} + \sum_l f_{AD+BC}^{(l)} J_{AD+BC}^{(l)} \quad (11)$$

where n and k run over the pairs within α and β sublattices, respectively, and l runs over the pairs across the two sublattices. Note that $f_{AB}^{(n)}$ and $f_{CD}^{(k)}$ include pairs in (AB and BA) and (CD and DC) configurations, respectively, while $f_{AD+BC}^{(l)}$ includes the cross-sublattice pairs exclusively in AD or BC configuration. By analogy with Eqs. (8) and (9) the Js are the differences between the excess energy of supercell structures with double defects of certain types and the excess energies of hypothetical supercells with the same defects at infinite separation. The energies of these hypothetical structures play the role of the effective parameters. Here we assume that in $MgSiO_3$–Al_2O_3 solid solutions with ilmenite and perovskite structures the mixing of Mg with Al and Si with Al occurs within separate sublattices, hereafter referred to as "Mg" and "Si". Three types of pairwise interactions can thus be distinguished: 1) the interaction MgMg + AlAl = 2AlMg within the "Mg" sublattice, 2) the interaction SiSi + AlAl = 2AlSi within the "Si"-sublattice, and 3) the cross-sublattice MgSi + AlAl = MgAl + SiAl interaction. To determine these interactions both in the "MgSi" and "AlAl" limits one needs to consider six types of double defects. To be able to determine all the six adjustable parameters (and thus the absolute values of all pairwise interactions) a few additional structures with quadruple Al_2Al_2 and Mg_2Si_2 defects were processed. Such structures, being charge neutral, contain both intra- and cross-sublattice defect pairs and thus their excess energies can be fitted together with the structures with the cross-sublattice double defects. The next sections describe the results of such calculations for perovskite and ilmenite. However, all calculated perovskite structures in the Al-rich side with MgSi defects were thermodynamically so unstable, that during optimization they transformed into another space group. Thus being unsuitable for the DDM fitting. In the Al-rich side, the corundum and Rh_2O_3(II) structure types are heavily favoured over the perovskite structure type. The total energy of the structures with such defects appeared lower than the energy of the mechanical mixture of $MgSiO_3$ and Al_2O_3 perovskites. Thus, in the perovskite case only MgSi-rich compositions have been considered. Consequently, we had to postulate that the mixing in perovskite is symmetric with respect to $x_{Al2O3} = 0.5$.

3. Ab initio calculations

Static density functional calculations were performed with the VASP (Vienna ab initio simulation package) code (Kresse and Furthmuller, 1996). The generalized gradient approximation (GGA) (Perdew et al., 1996) together with the projector augmented wave (Blöchl, 1994; Blöchl et al., 2003) method was used to calculate energies of the supercell structures at zero Kelvin and 25 GPa. In all calculations the following projector augmented wave (PAW) potentials were used: Core region cut-off radii are 1.5 a.u. for silicon (core configuration $1s^22s^2p^6$), 1.52 a.u. for oxygen (core configuration $1s^2$), 2.0 a.u. for magnesium (core configuration $1s^22s^2$) and 1.9 a.u for aluminium (core configuration $1s^22s^2p^6$).

A plane wave cut-off energy of 500 eV for all calculations proved to be reliable (convergence of the total energy to within 5×10^{-2} eV/f.u., convergence of pressure to within 0.4 GPa) and computationally acceptable. Energy differences converge to within 8×10^{-4} eV. For the Brillouin zone sampling the Monkhorst–Pack scheme (Monkhorst and Pack, 1976) was used, and convergence of energy and stress with respect to the mesh density was tested for each structure individually.

All perovskite and ilmenite structures were processed with a 160-atom (32 f.u.) and 120-atom (24 f.u.) supercells, respectively and the k-point sampling over a $2\times2\times2$ Monkhorst–Pack grid. The ions were relaxed with the conjugate gradient and the steepest descent methods. The energy minimizations proceeded until self-consistency within the prescribed tolerances (10^{-4} eV per unit cell for electronic optimization and 10^{-3} eV per unit cell for ionic relaxation) was reached. The cross-sublattice substitution does not change the charge of the supercell and thus, does not require charge neutralizing background corrections.

$$2Al^{3+} \leftrightarrow Mg^{2+}\ Si^{4+} \quad (12)$$

However, the determination of intra-sublattice interactions requires to consider the interactions within each of the sublattices separately:

$$2Al^{3+} \leftrightarrow Mg^{2+}\ Mg^{2+} + 2e \quad (13)$$

$$2Al^{3+} \leftrightarrow Si^{4+}\ Si^{4+} - 2e. \quad (14)$$

The resulting double-defect structures have an unbalanced charge. VASP allows to manually set the number of electrons, i.e. to change the valence of an atom in the calculations. The total negative charge is modeled as a homogeneous background charge. Coulomb interaction between the charged defects within the cell and the defects in its periodically arranged images changes the total energy of the system.

An analytical expression for the correction term (Leslie and Gillan, 1985; Karki and Khanduja, 2006):

$$\Delta E = -\frac{\alpha Q^2}{2\varepsilon_0 L}, \quad (15)$$

depends on is the lattice parameter, L, the Madelung constant, α, and the charge, Q. For a large supercell adopted here this value is of the order of 1 eV, which corresponds to about 30 meV/f.u. This exceeds the convergence errors by a factor of 10. However, the correction error is expected to be approximately the same for all structures with the same type of the double defect. Since only the relative energies of the double-defect structures are considered, the correction errors cancel out.

4. The Results

The main results are listed in Tables 1 and 2 and plotted in Figs. 1a–4b. The complete set of data is given in the Supplementary materials.

4.1. Perovskite solid solution

Fig. 1a shows the excess energy of the cross-sublattice AlAl defects in $MgSiO_3$ perovskite as the function of the distance between the Al atoms. The excess energies at all distances are positive. This means that the mixing enthalpy, at least in the vicinity of $MgSiO_3$, is positive. It is also certain that the placing of two Al defects close together costs less energy. Thus, the individual defects in the solid solution would tend to segregate. The dashed line in Fig. 1a defines "no interaction" limit. This would be the excess enthalpy of the double defect when the Al cations are placed at an infinitely large distance from each other. This energy is obtained by a fit to the excess energies of the double-defect structures using Eq. (1). The Js are calculated as the differences between the enthalpies of the structures with the double defects at given distances and the enthalpy at the "no interaction" limit. The fitting procedure uses the dual nature of the pairwise interactions: The Js are not only the ordering enthalpies, but also the "excess

Table 1
The comparison between the total and excess energies of the supercell structures of perovskite calculated with the DFT GGA and predicted with the *J*s-formalism (JF).

	DFT absolute	JF	DFT excess	JF
End-members				
$MgSiO_3$	−919.093	−919.093	0	0
Al_2O_3	−966.129	−966.129	0	0
Dist.	Double defects, AlAl in $MgSiO_3$			
2.717	−920.263	−920.263	0.453	0.453
2.836	−920.224	−920.224	0.512	0.512
2.960	−920.210	−920.210	0.533	0.533
3.203	−920.173	−920.173	0.588	0.588
5.338	−920.127	−920.127	0.657	0.657
5.354	−920.152	−920.152	0.620	0.620
5.421	−920.086	−920.086	0.719	0.719
5.493	−920.074	−920.074	0.738	0.738
5.553	−920.102	−920.102	0.696	0.696
5.618	−920.067	−920.067	0.749	0.749
5.601	−920.161	−920.161	0.606	0.606
5.750	−920.094	−920.094	0.707	0.707
7.162	−920.058	−920.058	0.761	0.761
7.174	−920.069	−920.069	0.745	0.745
7.224	−920.070	−920.070	0.743	0.743
7.360	−920.080	−920.080	0.728	0.728
Quadruple defect structures				
PQ1	−921.291	−921.254	1.119	1.174
PQ2	−921.119	−921.130	1.378	1.361
Disordered 50:50 structures				
PD	−939.544	−938.821	4.623	5.715
Ordered 50:50 structures				
PO1 (*P*1)	−944.768	−944.494	−3.251	−2.839
PO2 (*Pc*)	−945.425	−944.530	−4.241	−2.893
PO3 ($P\ \bar{1}$)	−944.133	−944.505	−2.295	−2.856
PO4 (*P*1)	−943.122	−944.184	−0.770	−0.864

The values are in eV per supercell containing 160 atoms. The excess energies are in kJ per one mole of the exchangeable atoms.

Table 2
The comparison between the total and excess energies of supercell structures of ilmenite calculated with the DFT GGA and predicted with the *J*s-formalism (JF).

	DFT absolute	JF	DFT excess	JF
End-members				
$MgSiO_3$	−690.642	−690.642	0	0
Al_2O_3	−741.212	−741.212	0	0
Dist.	Double defects, AlAl in $MgSiO_3$			
2.645	−691.913	−691.914	1.680	1.678
3.185	−691.877	−691.876	1.751	1.755
3.330	−691.845	−691.844	1.817	1.818
3.589	−691.852	−691.851	1.803	1.805
5.339	−691.707	−691.707	2.093	2.095
5.626	−691.809	−691.809	1.888	1.889
5.710	−691.751	−691.747	2.005	2.013
5.864	−691.639	−691.641	2.230	2.227
6.351	−691.560	−691.562	2.390	2.386
6.658	−691.542	−691.544	2.425	2.422
7.864	−691.546	−691.549	2.417	2.412
8.114	−691.554	−691.556	2.401	2.397
Dist.	Double defects, MgSi in Al_2O_3			
2.645	−738.296	−738.295	1.626	1.628
3.185	−738.198	−738.200	1.823	1.820
3.330	−738.203	−738.203	1.814	1.814
3.589	−738.199	−738.199	1.822	1.821
5.339	−738.058	−738.059	2.104	2.103
5.626	−738.163	−738.164	1.893	1.893
5.710	−738.024	−738.027	2.174	2.166
5.864	−738.037	−738.036	2.146	2.149
6.351	−737.970	−737.968	2.282	2.286
6.658	−737.953	−737.951	2.315	2.319
7.864	−737.963	−737.960	2.296	2.301
8.114	−737.972	−737.970	2.277	2.282
Quadruple defect structures				
IQ1	−735.346	−735.301	3.322	3.483
IQ2	−735.363	−735.364	3.287	3.369
IQ3	−693.169	−693.161	3.391	3.741
IQ4	−693.274	−693.275	3.179	3.533
Disordered 50:50 structure				
ID	−709.522	−709.636	12.875	12.821
Ordered 50:50 structure				
IO (*R*3)	−713.216	−713.870	5.450	3.536

The absolute energies are in eV per supercell containing 120 atoms. The excess energies are in kJ per one mole of the exchangeable atoms.

enthalpies", meaning that their integral effect, when it is summed proportionally to the numbers of pairs of dissimilar cations, gives the excess enthalpy of the configuration. Thus, the energy of "no interaction" limit is, in fact, the sum of the ordering interactions at all distances. This means that the enthalpy of the "no interaction" limit and the *J*s can be determined only together via a self consistent fitting procedure. Intra-sublattice *J*s, those which correspond to the ordering reactions MgMg + AlAl = 2MgAl and SiSi + AlAl = 2SiAl, also contribute to the excess enthalpies. The absolute values of these *J*s depend on the values of the effective parameters which correspond to the excess enthalpies of hypothetical structures with intra-sublattice defects at infinite separation. The problem is that, since the double-defect structures with the intra-sublattice double defects are not charge balanced, their excess enthalpies cannot be compared to those of the cross-sublattice defects and thus cannot be used in the fit. Consequently, there is insufficient data to simultaneously constrain the "no interaction" energy limits of the intra and cross-sublattice interactions. Therefore, we have calculated the excess energies of two structures with quadruple defects. The excess energies of these structures include intra-sublattice *J*s and thus all the adjustable parameters can be constrained. The results of the fit are shown in Fig. 1b and listed in Table 1. Fig. 1a shows that the intra-sublattice interactions have similar magnitude to those of the cross-sublattice ones. These interactions are generally negative, meaning that the "mixed-cation" pairs of MgAl- and SiAl-type are preferred at nearly all distances over the pairs with the same cations. The negative sign of these interactions can be understood noting that the electrostatic energy of two pairs of dissimilar cations is always lower than the sum of the energies of pairs composed of the same cations.

As a result of the DDM calculations we have obtained three sets of the *J* from which the excess enthalpy of any configuration can trivially be evaluated with Eq. (11) as a function of frequencies of pairs with dissimilar cations. This equation has been then used to simulate supercell structures with contrasting ordering states. By applying a Monte Carlo algorithm with the Metropolis sampling scheme (Metropolis et al., 1953) we could vary the cation distribution within the supercell and make it dependent on the temperature-like parameter. Such a simulation does not have true thermodynamic meaning, because the size of the supercell (64 exchangeable atoms) is too small. Nevertheless, it can be used to find ground states. By gradually decreasing the temperature within the supercell of the 50:50 composition we could find the ordered structure (Fig. 2) which has the space group symmetry *Pc*, and gives upon relaxation the lowest excess enthalpy (−4.241 kJ/mol with VASP, −2.893 kJ/mol with Eq. (11)). By slightly shifting the values of the *J*s we have found three additional ordered structures, two of which have the space group *P*1 and one the space group $P\bar{1}$. Due to the ordering the supercell size can be reduced. Thus, the atomic arrangements of all the four structures can be shown within a $1\times1\times2$ supercell. The atomic coordinates of these structures are given in the Supplementary materials. By setting the temperature equal to 100000 K, we simulated a structure with essentially disordered cation distribution. The static energies of the ordered and disordered structures were calculated with VASP and used to test the accuracy of Eq. (11). The predicted excess energies (in kJ/mole of 1/2 $MgSiO_3$) are compared to the DFT results in Table 1. Clearly, Eq. (11) performs well in predicting the excess enthalpies of the states with the contrasting ordering schemes.

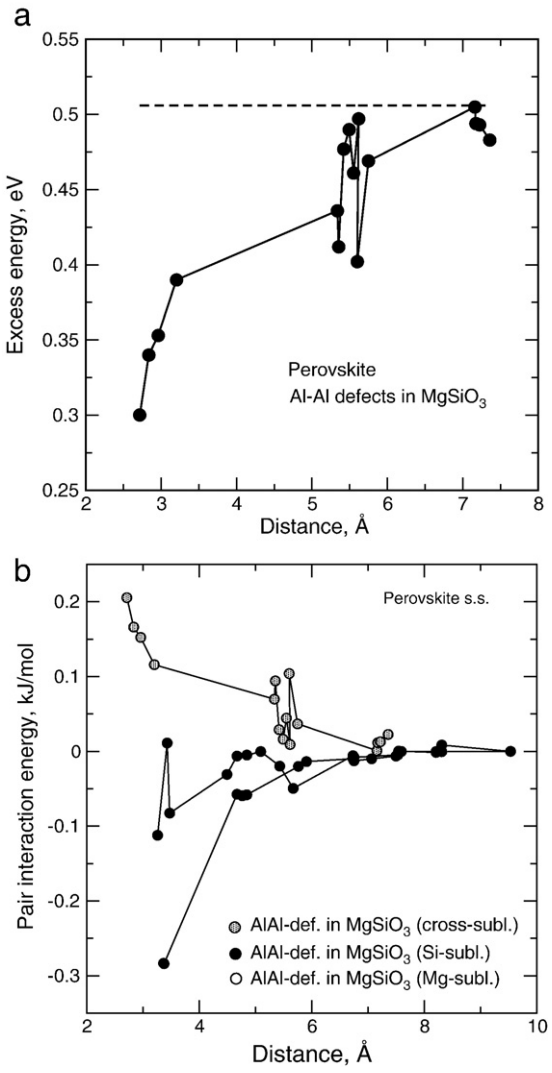

Fig. 1. a) The excess energies of the supercell structures with the AlAl defects in $MgSiO_3$ perovskite as the function of the distance between the individual defects. The dashed line corresponds to the "no interaction" limit, i.e. the enthalpy of a hypothetical structure with the defects placed at an infinitely large distance from each other. b) The pair-wise effective interactions in the perovskite solid solution recalculated from the energies of the double-defect structures.

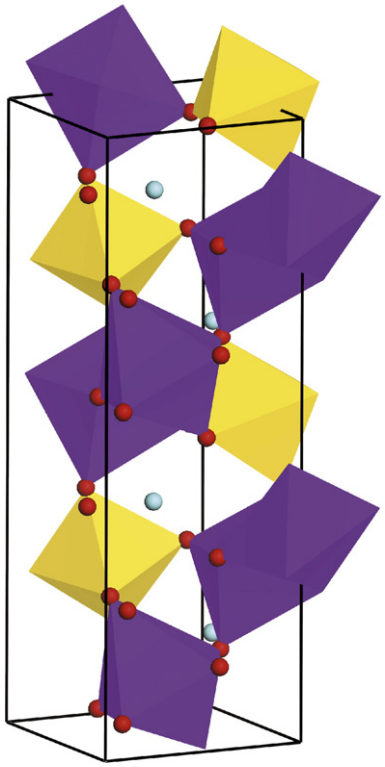

Fig. 2. The structure of the ordered intermediate compound, 50:50-2, with the lowest excess enthalpy shown in the $1\times1\times2$ supercell. It belongs to the *Pc* space group. The dark-yellow and pink polyhedra are filled with Si and Al atoms respectively, the Mg and O atoms are shown as light-blue and red balls, respectively.

4.2. Ilmenite solid solution

The DDM calculations for the ilmenite solid solution followed the scheme described for the perovskite. However, in this case we considered not only the AlAl defects in the $MgSiO_3$ host, but also MgSi defects in the Al_2O_3 corundum. Fig. 4a shows the excess energies of the defect structures with cross-sublattice defects as a function of the distance and the "no interaction" limits obtained with the least squares fit. To avoid the uncertainty of the "no interaction" limits of the intra-sublattice *J*s, four structures with quadruple defects were included in the fit. The complete set of the *J*s is plotted in Fig. 4b. Similarly to the perovskite case, Fig. 4a shows that the excess energies of the cross-sublattice defects are positive. The energies of the "no interaction" limits are much larger than those in perovskite. This means that in the limit of infinite dilution, when the defects are too far from each other to experience forces of ordering, the ilmenite solid solution has a much stronger tendency to phase separation than the perovskite. Fig. 4b shows that the *J*s in the both solid solutions show the similar pattern: the cross-sublattice interactions are positive and the intra-sublattice interactions are negative. To test the accuracy of Eq. (11) for the ilmenite, DFT calculations for structures with ordered (Fig. 3) and disordered configurations were performed. These structures were found with the procedures analogous to that described in the previous section. The coordinates of the ordered structure (space group *R*3) are given in the Supplementary materials. The excess enthalpy of this structure is higher than the mechanical mixture of $MgSiO_3$ and Al_2O_3 ilmenites. This metastable structure can be simulated only within a small supercell. The predicted excess energies of these structures are compared to the DFT results in Table 2.

5. Monte Carlo simulations

The double-defect calculations show that the mixing in the ilmenite solid solution is more non-ideal than for the perovskite. The calculations show also that the excess enthalpy in both solid solutions is composed of interactions of different strength. The large variance in the interaction energies implies the existence of strong ordering tendencies which might significantly affect the free energy of mixing at intermediate compositions and low temperatures. This implies that to be able to discuss the mixing quantitatively at any temperature and composition of interest one has to simulate the Boltzmann distribution of the configurational states. This has to be performed for a reasonably large supercell, because in small supercells the contribution from low-energy states is overestimated. Our experience shows that supercells containing 2–3 thousand of the exchangeable sites permit reliable estimates of the thermodynamic properties. For example, the predicted temperature of the order/disorder transition in dolomite becomes insensitive to the supercell size in supercells containing more than 2600 exchangeable sites (Vinograd et al., 2007a). Here we considered the supercells of perovskite and ilmenite containing 4096 and 3072 sites respectively.

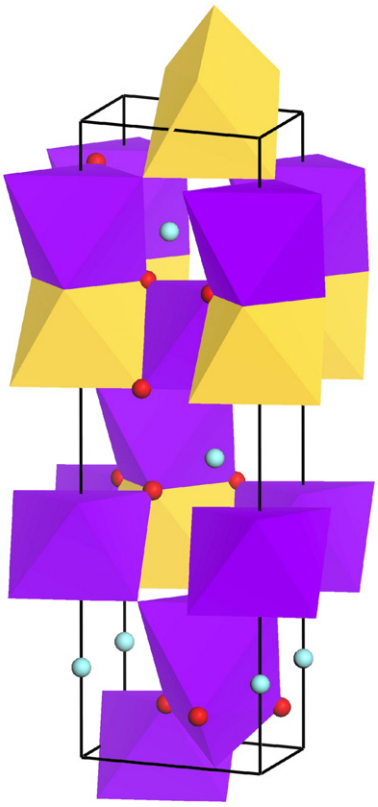

Fig. 3. The structure of the ordered intermediate ilmenite compound *R*3 with the lowest excess enthalpy. The dark-yellow and pink polyhedra are filled with Si and Al atoms respectively, the Mg and O atoms are shown as light-blue and red balls, respectively.

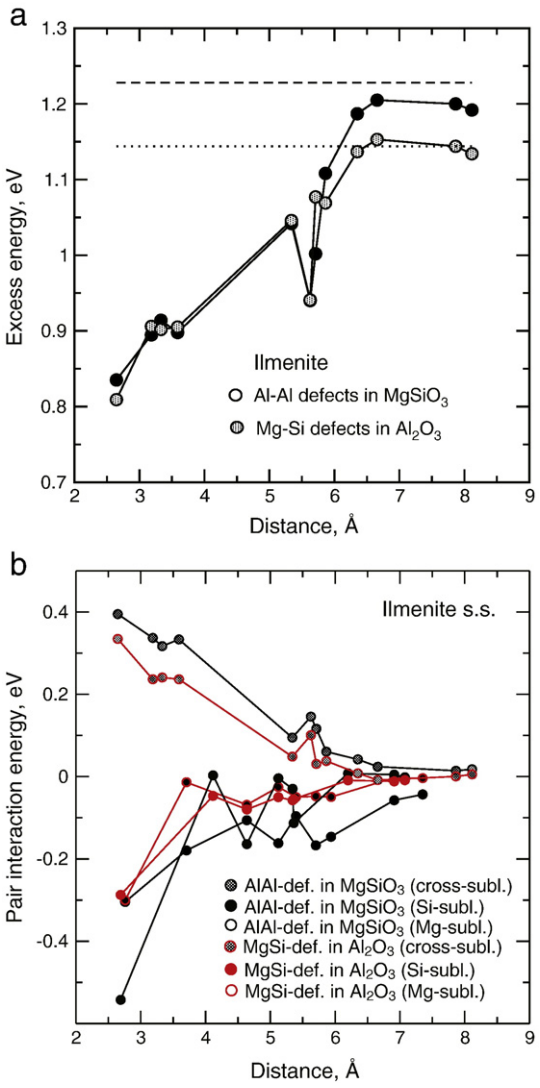

Fig. 4. a) The pair-wise effective interactions in the perovskite solid solution. b) The pair-wise effective interactions in the perovskite solid solution.

The temperature was varied in the intervals 373–2673 K and 1373–2673 K for perovskite and ilmenite, respectively, with a step of 100 K. The composition was varied with the steps of 0.03125 for perovskite and 0.04167 for ilmenite. The number of Monte Carlo steps in each run was 3×10^7 and only the last 1.5×10^7 steps were used in the averaging. The free energies of mixing were calculated with the method of thermodynamic integration (Warren et al., 2001), where the properties of the system are, at first, simulated in the state of complete disorder ($\lambda=0$) and then are gradually driven to the equilibrium at a given temperature by increasing the value of λ. Each point in the temperature–composition space was therefore simulated not only with the nominal values of the *J*s, but also with the *J*s scaled with the λ parameter. λ was varied in the interval 0–1 with a step of 0.04.

$$\Delta G = \Delta G_0 + \int_0^{\lambda} \Delta H_{\lambda} d\lambda, \tag{16}$$

where ΔH_λ is the average excess enthalpy of the supercell summed over the states, which correspond to a given value of λ and ΔG_0 is the free energy of mixing of the solid solution per 1 mol of exchangeable atoms in the state of complete disorder:

$$\Delta G_0 = H_0 + RT(x_{\mathrm{Mg}} ln(x_{\mathrm{Mg}}) + x_{\mathrm{Al}} ln(x_{\mathrm{Al}})), \tag{17}$$

where H_0 is obtained from Eq. (11) by substituting $f_{ij}^{(n)}$ with values proportional to the probabilities of finding *IJ* pairs in the completely random mixture.

The enthalpy isotherms in perovskite and ilmenite are shown in Fig. 5a and b, respectively. The Gibbs free energies of mixing are plotted in Fig. 6a and b. The configurational entropies were calculated from the enthalpies and free energies of mixing with the relation:

$$\Delta S = (\Delta H - \Delta G)/T. \tag{18}$$

These functions are plotted in Fig. 7a and b.

6. Activity–composition relations

To simplify applications of the calculated free energy functions in petrological studies we have fitted them in the intervals of 1673–2673 K with the Redlich–Kister polynomials:

$$G_{\mathrm{excess}} = x_1 x_2 \sum_{i=0}^{n} A_i (x_1 - x_2)^i, \tag{19}$$

where A_i are further expanded as functions of temperature $A_i = A_i^h - TA_i^s$ and x_1 is the mole fraction of Al_2O_3.

The coefficients of these polynomials are given in Table 3. The free energy values nominally correspond to 25 GPa. We assume, however, that the models can be used in a wider pressure interval (20–30 GPa). Our experience with other oxide solid solution systems shows that changes in the pressure of the order of 5 GPa do not significantly affect

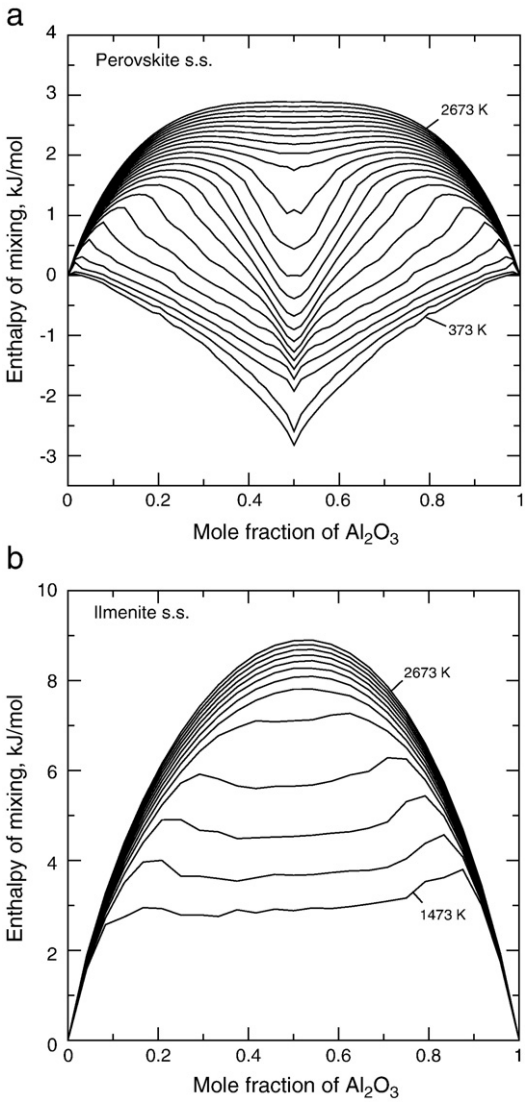

Fig. 5. a) The enthalpy of mixing isotherms in the perovskite solid solution simulated with the Monte Carlo method. b) The enthalpy of mixing isotherms in the ilmenite solid solution simulated with the Monte Carlo method.

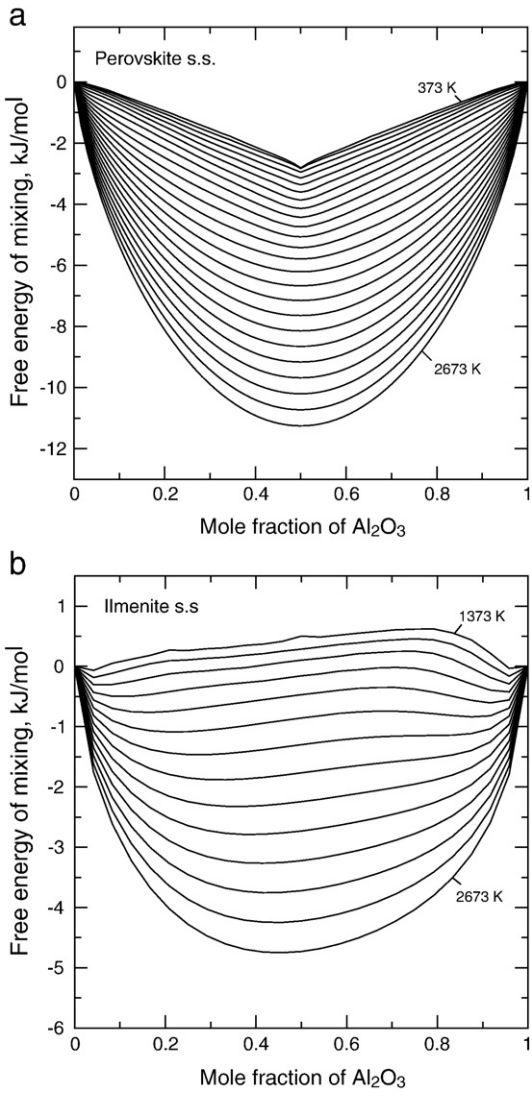

Fig. 6. a) The Gibbs free energy of mixing isotherms in the perovskite solid solution simulated with the Monte Carlo method. b) The Gibbs free energy of mixing isotherms in the ilmenite solid solution simulated with the Monte Carlo method.

the thermodynamic mixing functions. These polynomials are used in the next section to calculate the thermodynamic activities of $MgSiO_3$ and Al_2O_3 components in perovskite and ilmenite phases in equilibrium with garnet.

7. Phase equilibrium calculations in MAS

The derived thermodynamic models were applied to calculate phase equilibria of perovskite, ilmenite and garnet in the MAS system in the pressure interval of 20–30 GPa. The activity–composition model of the pyrope–majorite solid solution in the garnet phase was adopted from the study of Vinograd et al. (2006). The standard thermodynamic properties of the end-members were taken from the data base of Fabrichnaya (1999). The calculations were performed with the Thermo-Calc program (Andresson et al., 2002). The use of the new activity–composition models requested an adjustment of the standard enthalpy of Al_2O_3 perovskite. The new value is 10 kJ higher than that in data base (Fabrichnaya, 1999).

The results of the calculations at 1873, 2023 and 2273 K are shown in Figs. 8–10, respectively. The predicted pressures of the reaction perovskite + corundum = garnet are 0.5 GPa lower than those determined in the experiments of Kubo and Akaogi (2000) and 2 GPa higher than those of the experimental data of Hirose et al. (2001). Calculations of garnet decomposition pressure at 1773 K show good agreement with the results of Irifune et al. (1996). The comparison of the results of Hirose et al. (2001) with the above mentioned experimental data indicates a systematic shift of about 2.5 GPa to lower pressures.

8. Discussion and conclusions

The present study is consistent in general with the conclusion of Panero et al. (2006) that the deviation from ideal mixing, measured in terms of regular model, in the ilmenite solid solution is much greater than in the perovskite phase. However, in detail, our simulations show that both phases reveal a more complex mixing behaviour. In the perovskite solid solution the enthalpy of mixing is greatly decreased at the intermediate composition due to the stabilization of the ordered phase. The decrease in the enthalpy of mixing due to the ordering is associated with a decrease in the configurational entropy. The entropy isotherms, both in the perovskite and ilmenite cases, deviate significantly from the ideal mixing curve (Fig. 7a and b). Thus, both solid solutions obey regular mixing only in the high-temperature

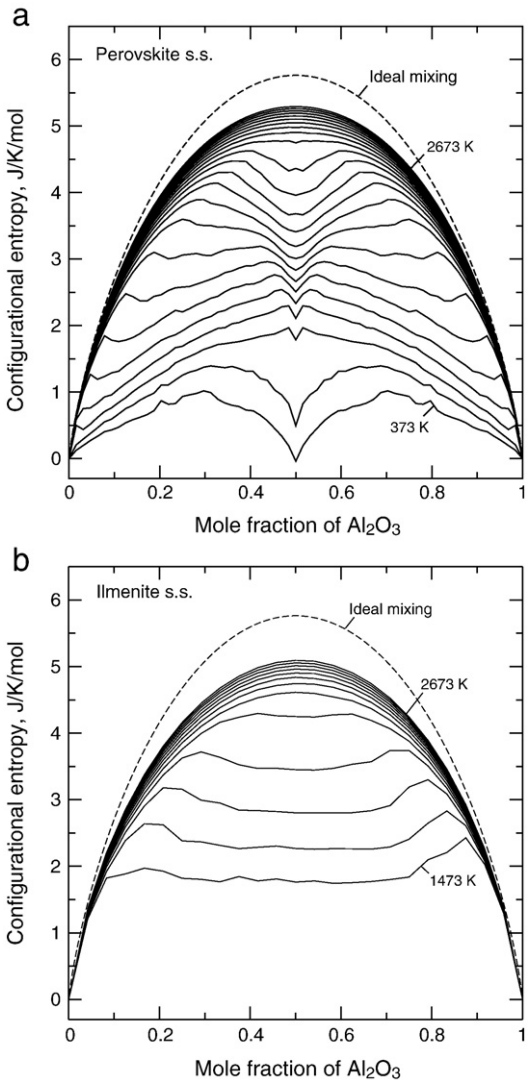

Fig. 7. a) The configurational entropy isotherms in the perovskite solid solution calculated with the thermodynamic integration method. b) The configurational entropy isotherms in the ilmenite solid solution calculated with the thermodynamic integration method.

limit. This prediction is at variance with the conclusion of Panero et al. (2006) that the entropy in the both solutions is essentially ideal. Panero et al. (2006) have arrived at this conclusion following the approach of Akber-Knutson and Bukowinski (2004) where thermodynamic mixing properties of a solid solution are evaluated by sampling a small subset of the accessible states. Panero et al. (2006) considered a subset of 2000 randomly chosen configurations within $\sim 3.8\times10^8$ available for a 120 atoms supercell and assumed their energy distribution to be representative for the whole set. The energies of individual configurations were calculated with a force-field model. The problem is, that this approach is bound to predict a nearly ideal entropy because the probability distribution function has a sharp maximum at the average enthalpy and thus there is a very high probability that the energies of the configurations sampled at random will be very close to the average value. When the enthalpies of the sampled configurations (and thus their probabilities) deviate little of each other, the entropy of the subset approaches the maximum. The Monte Carlo approach does not have such a drawback.

Consistently with the earlier study of Yamamoto et al. (2003), we find that the excess enthalpies of the cross-sublattice double defects

Table 3
The parameters of Redlich–Kister polynomials for the excess free energy of mixing in perovskite and ilmenite solid solutions.

i	A_i^h (J/mol)	A_i^s (J/K/mol)
Perovskite s.s.		
0	29,339	−5.4
1	2001	−0.0373
2	12,921	+1.8132
3	4855	+3.4275
Ilmenite s.s.		
0	9235	−2.759
2	12,564	+2.642
4	−1115	−0.937

The values are per $AlO_{1.5}$ formula unit.

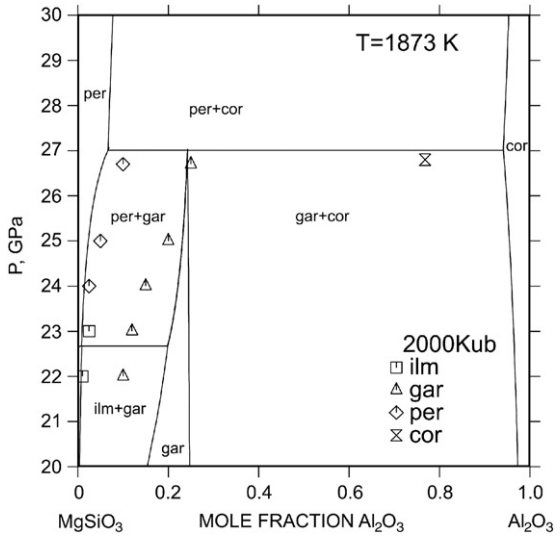

Fig. 8. Calculated phase diagram of the $MgSiO_3$ and Al_2O_3 system at 1873 K using the activity–composition models derived in this study. The properties of the pure phases are adopted from the data base of Fabrichnaya (1999) Symbols are phase compositions determined by EPMA analysis (Kubo and Akaogi, 2000).

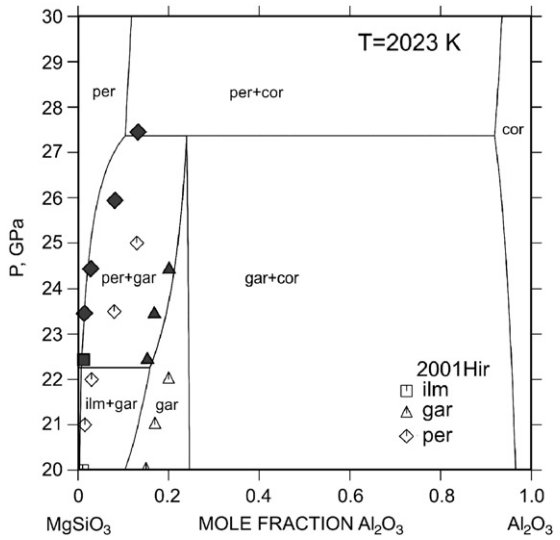

Fig. 9. Calculated phase diagram of the $MgSiO_3$ and Al_2O_3 system at 2023 K. Empty symbols are phase compositions determined by monitoring changes of XRD and Raman spectra (Hirose et al., 2001). Filled symbols are data from Hirose et al. (2001) corrected by 2 GPa to be consistent with phase transformations in pure $MgSiO_3$ (Fabrichnaya, 1999).

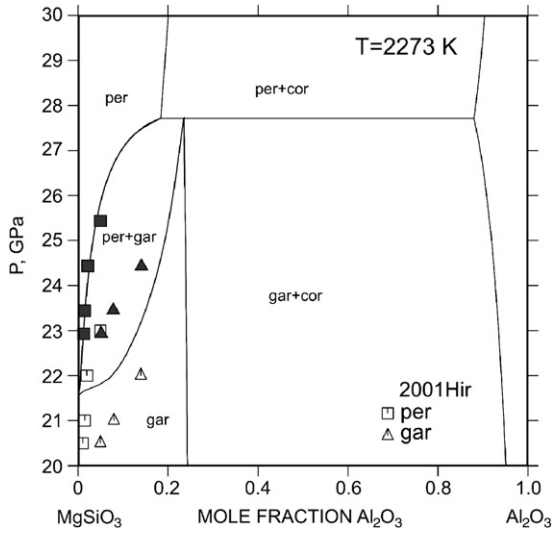

Fig. 10. The phase relations in the MAS system at 2273 K. Symbols are the same as in Fig. 9.

are smaller at short interatomic distances. When the distance between the defects increases, the excess enthalpies approach a higher value, which we call the "non-interaction" limit (Figs. 1a and 4a). This is the enthalpy of mixing not perturbed by ordering. This limit is reached at an infinitely high temperature, when the difference in the excess enthalpies of the double-defect structures is incomparably small relative to the temperature factor. The system in this state obeys regular mixing. The excess enthalpy in the regular limit can be estimated by calculating the excess energies of the double structures with the defects at the maximum possible distance. On the contrary, when one aims to estimate the enthalpy in the low-temperature limit, one should use the excess energy of a double-defect structure with the lowest excess energy. In the cases of perovskite and ilmenite these are the structures with the defects at the shortest distance. To assess the mixing behaviour at a given temperature one needs to sum the contributions from all double defects according to the Boltzmann factors. However, one should keep in mind that this weighting will not give an accurate result because the supercell is too small to provide correct statistics. The only sensible alternative is to increase the supercell and to use a Monte Carlo algorithm. Attempts to estimate mixing enthalpy from the double defects without the use of the Monte Carlo method are futile.

Random sampling approaches, when they applied to intermediate compositions, permit to estimate the enthalpy in the high-temperature limit only. Our values for the excess enthalpy of the disordered 50:50 structures in perovskite and ilmenite at 25 GPa are 4.623 and 12.875 kJ per formula unit with one cation, respectively (Tables 1 and 2). These values when recalculated to eV per formula unit with two cations (0.096 and 0.267 eV) are marginally consistent with the values reported by Panero et al. (2006) (Fig. 5a in Panero et al., 2006) which are of the order of 0.06 and 0.20 eV, respectively. The values obtained by Panero et al. (2006) are slightly lower consistently with their strategy to plot the lowest values found for each composition. We should note also that our model of the perovskite solid solution cannot be compared to the recent result of Tsuchiya and Tsuchiya (2008) obtained with the random sampling approach. This is due to the fact, that we considered perovskite as an isostructural solid solution, while Tsuchiya and Tsuchiya (2008) treated is as a "crossover" between perovskite and Rh_2O_3 end members.

The DDM coupled with the Monte Carlo algorithm allows to map the functions of mixing within a wide temperature interval. No a priori assumption of regular mixing was required. The method makes it possible to investigate the most likely ordering schemes by direct sampling of the most important pairwise interactions. We find that the cross-sublattice interactions in both phases are positive showing that the AlAl and MgSi pairs are preferred over the AlMg and AlSi pairs at all distances. Since the formation of some AlMg and AlSi pairs is unavoidable due to mixing, there is always a positive contribution to the excess enthalpy. On the other hand, the inter-sublattice interactions are negative showing that the AlSi and AlMg pairs are always preferred over the AlAl + SiSi and AlAl + MgMg groupings, respectively. This creates the possibility of decreasing the enthalpy of mixing due to the ordering of Al,Si and Al,Mg within the sublattices. Such an ordering is particularly effective at intermediate compositions where the numbers of AlSi and AlMg groupings increase. When the effects of the ordering within the sublattices overcome the effect of the increase in the number of AlMg and AlSi pairs across the sublattices, an ordered phase can form.

Even though the signs and the magnitudes of the ordering interactions in perovskite and ilmenite are similar, the phase relations are very different. In ilmenite the tendency to demixing prevails. The difference in the ordering behaviour of the two solutions is certainly related to the different structure types. We observe that in the ilmenite structure the numbers of the cross-sublattice AlSi and AlMg pairs introduced by a single defect pair at the second, third and fourth nearest-neighbor distances are three times larger than in the perovskite structure. This suggests that it is generally more difficult to avoid the formation of the unfavorable cross-sublattice interactions in the ilmenite phase.

Our study allows also to estimate the degree of asymmetry of the mixing functions. The similarity between the fitted values of the excess enthalpies in the limit of infinite separation computed for the double-defect structures with the contrasting compositions suggests that the asymmetry in the ilmenite phase is small. It is interesting to observe that the peculiar shape of the excess enthalpy of the AlAl defects in $MgSiO_3$ vs. the defect separation is reproduced nearly exactly with the MgSi defects in Al_2O_3 (Fig. 4a). This similarity is probably due to the fact that AlAl pair in the $MgSiO_3$ host and the MgSi pair in the Al_2O_3 host experience approximately the same structural tension due to the same misfit between the same combination of the cations. It is conceivable that the same similarity would exist in the perovskite phase, if the MgSi defects in Al_2O_3 were stable. This supports the present symmetric treatment of the perovskite solid solution.

The predicted phase separation in the ilmenite phase is consistent with the experimental phase relations at high pressures in MAS, which require the existence of two ilmenites with contrasting compositions (Fig. 9). On the other hand, the phase relations are consistent with the existence of only one perovskite phase. The ease with which the experimental phase relations can be fitted with the new mixing models shows that the presently simulated excess effects are reasonable. These models are recommended to be used in petrological calculations.

The most important conclusion of this study is that with the implementation of the DDM the already available computational resources appear to be sufficient for the calculation of mixing effects in complex petrologically relevant phases with ab initio accuracy. This opens the perspective of creation of internally consistent thermodynamic data bases for petrological materials with externally parameterized mixing models. Such data bases could gradually substitute the currently available ones, in which the standard properties of pure phases and the parameters of mixing models are assessed together with the effect of strong correlation between these types of data and, consequently, their low accuracy.

Acknowledgements

We thank the CSCS Swiss National Supercomputing Centre and ETH Zurich for the use of supercomputers. VVL acknowledges the support from the Helmholtz Society (grant VH-VI 313).

Appendix A. Supplementary data

Supplementary data associated with this article can be found, in the online version, at doi:10.1016/j.epsl.2010.04.026.

References

Akber-Knutson, S., Bukowinski, M.S.T., 2004. The energetics of aluminum solubility into $MgSiO_3$ perovskite at lower mantle conditions. Earth Planet. Sci. Lett. 220 (3–4), 317–330 Apr.

Andresson, J.O., Helander, T., Höglund, L., Shi, P., Sundman, B., 2002. The Thermo-Calc and Dictra, computational tools for materials science. Calphad 26, 273–312.

Austen, K., Wright, K., Slater, B., Gale, J.D., 2005. The interaction of dolomite surfaces with metal impurities: a computer simulation study. Phys. Chem. Chem. Phys. 7, 4150–4156.

Becker, U., Pollok, K., 2002. Molecular simulations of interfacial and thermodynamic mixing properties of the grossular–andradite garnets. Phys. Chem. Miner. 29, 52–64.

Becker, U., Fernandez-Gonzalez, A., Prieto, M., Harrison, R., Putnis, A., 2000. Direct calculation of thermodynamic properties of the barite/celectite solid solution from molecular principles. Phys. Chem. Miner. 27, 291–300.

Blöchl, P.E., 1994. Projector augmented-wave method. Phys. Rev. B 50 (24), 17953–17979.

Blöchl, P.E., Forst, C.J., Schimpl, J., 2003. Projector augmented wave method: ab initio molecular dynamics with full wave functions. Bull. Mater. Sci. 26 (1), 33–41.

Bosenick, A., Dove, M.T., Geiger, C.A., 2000. Simulation studies on the pyrope–grossular garnet solid solution. Phys. Chem. Miner. 27 (6), 398–418 Jun.

Connolly, J.W.D., Williams, A.R., 1983. Density-functional theory applied to phase transformations in transition-metall alloys. Phys. Rev. B 27 (8), 5169–5172.

Fabrichnaya, O.B., 1999. The phase relations in the FeO–MgO–Al_2O_3–SiO_2 system: assessment of thermodynamic properties and phase equilibria at pressures up to 30 GPa. Calphad 21 (1), 19–67.

Gale, J.D., 1997. Gulp—a computer program for the symmetry adapted simulation of solids. J. Chem. Soc.: Faraday Trans. 93, 629–637.

Gale, J.D., Rohl, A.L., 2003. The General Utility Lattice Program (GULP). Mol. Simul. 29, 291–341.

Goldsmith, J.R., Heard, H.C., 1961. Subsolidus phase relations in the system. J. Geol. 69, 45–74.

Hirose, K., Fei, Y.W., Ono, S., Yagi, T., Funakoshi, K., 2001. In situ measurements of the phase transition boundary in $Mg_3Al_2Si_3O_{12}$: implications for the nature of the seismic discontinuities in the earth's mantle. Earth Planet. Sci. Lett. 184 (3–4), 567–573 Jan.

Hoshino, T., Schweika, W., Zeller, R., Dederichs, P.H., 1993. Impurity–impurity interactions in Cu, Ni, Ag, and Pd. Phys. Rev. B 47 (9), 5106–5117.

Irifune, T., Koizumi, T., Ando, J., 1996. An experimental study of the garnet–perovskite transformation in the system $MgSiO_3$–$Mg_3Al_2Si_3O_{12}$. Phys. Earth Planet. Inter. 96, 147–157.

Karki, B.B., Khanduja, G., 2006. Computer simulation and visualization of vacancy defects in $MgSiO_3$ perovskite. Model. Simul. Mater. Sci. Eng. 14 (6), 1041–1052 Sep.

Kresse, G., Furthmuller, J., 1996. Efficient iterative schemes for ab initio total-energy calculations using a plane-wave basis set. Phys. Rev. B 54 (16), 11169–11186.

Kubo, A., Akaogi, M., 2000. Post-garnet transitions in the system $Mg_4Si_4O_{12}$–$Mg_3Al_2Si_3O_{12}$ up to 28 GPa: phase relations of garnet, ilmenite and perovskite. Phys. Earth Planet. Inter. 121, 85–102.

Leslie, M., Gillan, M.J., 1985. The energy and elastic dipole tensor of defects in ionic-crystals calculated by the supercell method. J. Phys. C-Solid State Phys. 18 (5), 973–982.

Metropolis, N., Rosenbluth, A.W., Rosenbluth, M.N., Teller, A.H., Teller, E., 1953. Equation of state calculations by fast computing machines. J. Chem. Phys. 21, 1087–1092.

Monkhorst, H.J., Pack, J.D., 1976. Special points for Brillouin-zone integrations. Phys. Rev. B 13, 5188–5192.

Palin, E.J., Harrison, R.J., 2007. A Monte Carlo investigation of the thermodynamics of cation ordering in 2–3 spinels. Am. Mineralog. 92, 1334–1345.

Panero, W.R., Akber-Knutson, S., Stixrude, L., 2006. Al_2O_3 incorporation in $MgSiO_3$ perovskite and ilmenite. Earth Planet. Sci. Lett. 252 (1–2), 152–161 Nov.

Perdew, J.P., Burke, K., Ernzerhof, M., 1996. Generalized gradient approximation made simple. Phys. Rev. Lett. 77 (18), 3865–3868.

Sanchez, J.M., Ducastelle, F., Gratias, D., 1984. Generalized cluster description of multicomponent systems. Phys. A 128 (1–2), 334–350.

Stebbins, J.F., Kojitani, H., Akaogi, M., Navrotsky, A., 2003. Aluminum substitution in $MgSiO_3$ perovskite: investigation of multiple mechanisms by Al-27 NMR. Am. Mineralog. 88 (7), 1161–1164 Jul.

Tsuchiya, J., Tsuchiya, T., 2008. Postperovskite phase equilibria in the $MgSiO_3$–Al_2O_3 system. Proc. Natl. Acad. Sci. U. S. A. 105 (49), 19160–19164.

Vinograd, V.L., Sluiter, M.H.F., 2006. Thermodynamics of mixing in pyrope–grossular, $Mg_3Al_2Si_3O_{12}$–$Ca_3Al_2Si_3O_{12}$, solid solution from lattice dynamics calculations and Monte Carlo simulations. Am. Mineralog. 91, 1815–1830.

Vinograd, V.L., Sluiter, M.H.F., Winkler, B., Putnis, A., Halenius, U., Gale, J.D., Becker, U., 2004. Thermodynamics of mixing and ordering in the pyrope–grossular solid solution. Mineralog. Mag. 68, 101–121.

Vinograd, V.L., Winkler, B., Putnis, A., Kroll, H., Milman, V., Gale, J.D., Fabrichnaya, O.B., 2006. Thermodynamics of pyrope–majorite, $Mg_3Al_2Si_3O_{12}$–$Mg_4Si_4O_{12}$, solid solution from atomistic model calculations. Mol. Simul. 32, 85–99.

Vinograd, V.L., Burton, B.P., Gale, J.D., Allan, N.L., Winkler, B., 2007a. Activity–composition relations in the system $CaCO_3$–$MgCO_3$ predicted from static structure energy calculations and Monte Carlo simulations. Geochim. Cosmochim. Acta 225, 304–313.

Vinograd, V.L., Winkler, B., Gale, J.D., 2007b. Thermodynamics of mixing in diopside-jadeite, $CaMgSi_2O_6$–$NaAlSi_2O_6$, solid solution from static lattice energy calculations. Phys. Chem. Miner. 34, 713–725.

Vinograd, V.L., Sluiter, M.H., Winkler, B., 2009. Subsolidus phase relations in the $CaCO_3$–$MgCO_3$ system predicted from the excess enthalpies of supercell structures with single and double defects. Phys. Rev. B 79, 104201–104209.

Walter, M.J., Tronnes, R.G., Armstrong, L.S., Lord, O.T., Caldwell, W.A., Clark, S.M., 2006. Subsolidus phase relations and perovskite compressibility in the system MgO–$AlO_{1.5}$–SiO_2 with implications for Earth's lower mantle. Earth Planet. Sci. Lett. 248 (1–2), 77–89 Aug.

Warren, M.C., Dove, M.T., Myers, E.R., Bosenick, A., Palin, E.J., Sainz-Diaz, C.I., Guiton, B.S., Redfern, S.A.T., 2001. Monte Carlo methods for the study of cation ordering in minerals. Mineralog. Mag. 65 (2), 221–248 Apr.

Yamamoto, T., Yuen, D.A., Ebisuzaki, T., 2003. Substitution mechanism of Al ions in $MgSiO_3$ perovskite under high pressure conditions from first-principles calculations. Earth Planet. Sci. Lett. 206, 617–625.

Zhang, F.W., Oganov, A.R., 2006. Mechanisms of Al^{3+} incorporation in $MgSiO_3$ post-perovskite at high pressures. Earth Planet. Sci. Lett. 248 (1–2), 69–76 Aug.